Appendix

Derivation of KCNQ1 and I_{Ks} Models

Activation

This section describes the rationale for the model structure; it follows model development for the *Shaker* K^+ channel by Zagotta, Hoshi and Aldrich [1].

The transition between two energetic states of a channel can be modeled as following:

$$R \underset{\beta}{\overset{\alpha}{\rightleftharpoons}} A$$

Assuming that the rates are exponentially dependent on voltage, they are described by these equations.

$$\alpha = \alpha_0 \cdot \exp\left(z_\alpha \cdot \frac{V_m \cdot F}{R \cdot T}\right)$$
$$\beta = \beta_0 \cdot \exp\left(-z_\beta \cdot \frac{V_m \cdot F}{R \cdot T}\right)$$

α_0 and β_0 (ms) are the transition rates when $V_m = 0$ mV.
z_α and z_β (C) are the equivalent charge movements during the state transition.

$$F = 96485 \ \frac{\text{C}}{\text{mol}} \quad \textbf{(Faraday Constant)}$$
$$R = 8314 \ \frac{\text{J}}{\text{kmol} \cdot \text{K}} \quad \textbf{(Gas Constant)}$$
$$T = 310 \text{ K} \quad \textbf{(Body Temperature)}$$

The model describes two transitions for each of four voltage sensors. If a single transition for a single voltage sensor is $R \underset{\beta}{\overset{\alpha}{\rightleftharpoons}} A$, then the following describes two transitions for a single voltage sensor. R_1 and R_2 are resting positions; A is the activated position.

$$R_1 \underset{\beta}{\overset{\alpha}{\rightleftharpoons}} R_2 \underset{\delta}{\overset{\gamma}{\rightleftharpoons}} A$$

This presentation can be extended to four voltage sensors as in Zagotta et al ([1]. The channel is open when all four voltage sensors are in the activated position.

$$\left.\begin{array}{l} R_1 \underset{\beta}{\overset{\alpha}{\rightleftharpoons}} R_2 \underset{\delta}{\overset{\gamma}{\rightleftharpoons}} A \\ R_1 \underset{\beta}{\overset{\alpha}{\rightleftharpoons}} R_2 \underset{\delta}{\overset{\gamma}{\rightleftharpoons}} A \\ R_1 \underset{\beta}{\overset{\alpha}{\rightleftharpoons}} R_2 \underset{\delta}{\overset{\gamma}{\rightleftharpoons}} A \\ R_1 \underset{\beta}{\overset{\alpha}{\rightleftharpoons}} R_2 \underset{\delta}{\overset{\gamma}{\rightleftharpoons}} A \end{array}\right\} \textbf{Open}$$

Since each voltage sensor is assumed to move independently, the open probability is the occupancy in A to the fourth power (A^4). These transitions can also be described by a fifteen closed-state Markov model (for each permutation of voltage sensor positions described below), which should be used when there are transitions that depend on open state occupancy. The presence of transitions that depend on open-state occupancy makes the activation transitions dependent on each other, not allowing the simplification of A^4 that applies only to independent transitions. The Markov representation is used in the models of I_{Ks} and KCNQ1 and accounts for C_1 thru C_{15} as shown in **Figure 1** of the paper. Each closed state represents a permutation of voltage sensor positions. For example, C_1 is the energetic state where all four sensors are in R_1. The transition rate from C_1 to C_2, where one sensor is in R_2 and three sensors are in R_1, is $4 \cdot \alpha$ since movement of any one of four sensors from R_1 to R_2 can change the channel state from C_1 to C_2. The transition from C_2 to C_6 has the rate γ because only one sensor can transition from R_2 to A. When all four sensors are in the activated position C_{15}, the channel is able to transition to the open state.

The large number of transitions before opening generates a delay before activation, while the symmetry of the model (four identical voltage sensors) requires only four transition rates to describe the process.

Koren et al [2] have described a voltage-independent transition before the open state for RCK1, as revealed by pulses to highly negative potentials that do not increase the rate of deactivation. Unpublished data (J. Cui) suggest that such a voltage-independent transition exists also for I_{Ks} and KCNQ1. The final model of activation is shown below. Experiments were best fit with a voltage-independent transition into the open state and a voltage-dependent transition in the reverse direction, from the open to closed state.

$$\left.\begin{array}{l} R_1 \underset{\beta}{\overset{\alpha}{\rightleftharpoons}} R_2 \underset{\delta}{\overset{\gamma}{\rightleftharpoons}} A \\ R_1 \underset{\beta}{\overset{\alpha}{\rightleftharpoons}} R_2 \underset{\delta}{\overset{\gamma}{\rightleftharpoons}} A \\ R_1 \underset{\beta}{\overset{\alpha}{\rightleftharpoons}} R_2 \underset{\delta}{\overset{\gamma}{\rightleftharpoons}} A \\ R_1 \underset{\beta}{\overset{\alpha}{\rightleftharpoons}} R_2 \underset{\delta}{\overset{\gamma}{\rightleftharpoons}} A \end{array}\right\} \underset{\eta}{\overset{\theta}{\rightleftharpoons}} \textbf{Open}$$

Open State Transitions

KCNQ1 channels show a delay before inactivation as well as varying rates of deactivation that depend on pulse duration (**Figure 2E and 2F in paper**). Experiments show that the minimal number of open states is two, based on the delay and varying rates of deactivation [3,4]. However, to account quantitatively for deactivation rate as well as delay, five open states were necessary. These states could possibly account for four independent transitions of the channel subunits after the channel is open, as shown below. The transition rates are analogous to the activation transition rates.

Early open states $\left\{ \begin{array}{l} O_a \underset{\omega}{\overset{\psi}{\rightleftharpoons}} O_b \\ O_a \underset{\omega}{\overset{\psi}{\rightleftharpoons}} O_b \\ O_a \underset{\omega}{\overset{\psi}{\rightleftharpoons}} O_b \\ O_a \underset{\omega}{\overset{\psi}{\rightleftharpoons}} O_b \end{array} \right\}$ **Late open states**

$$\Downarrow$$

$$O_1 \underset{\omega}{\overset{4\psi}{\rightleftharpoons}} O_2 \underset{2\omega}{\overset{3\psi}{\rightleftharpoons}} O_3 \underset{3\omega}{\overset{2\psi}{\rightleftharpoons}} O_4 \underset{4\omega}{\overset{\psi}{\rightleftharpoons}} O_5$$

Even with the additional open states a sufficient delay was not achieved. To increase the delay, negative cooperativity was introduced in the model. This was accomplished, as in Zagotta, Hoshi and Aldrich [1], by

$$x_\psi = \exp(z_\psi \cdot (z_\psi + z_\omega) \cdot \nu \cdot \frac{F}{RT})$$

$$x_\omega = \exp(z_\omega \cdot (z_\psi + z_\omega) \cdot \nu \cdot \frac{F}{RT})$$

$$O_1 \underset{\omega \cdot x_\omega^0}{\overset{4\psi \cdot x_\psi^0}{\rightleftharpoons}} O_2 \underset{2\omega \cdot x_\omega^1}{\overset{3\psi \cdot x_\psi^1}{\rightleftharpoons}} O_3 \underset{3\omega \cdot x_\omega^2}{\overset{2\psi \cdot x_\psi^2}{\rightleftharpoons}} O_4 \underset{4\omega \cdot x_\omega^3}{\overset{\psi \cdot x_\psi^3}{\rightleftharpoons}} O_5$$

In **Figure 1** of the paper, these transitions are abbreviated as:

$$\psi_n = \psi \cdot x_\psi^{n-1}, \quad \omega_n = \omega \cdot x_\omega^{n-1}$$

The I_{Ks} model closely resembles the KCNQ1 model with fifteen closed states that are derived from the theory described above. However, I_{Ks} has fewer open state transitions (only two open states) and no inactivation. Experimental evidence, described below, provides some indication of the difference between KCNQ1 and I_{Ks} open state transitions and the nature of inactivation.

KCNQ1 open states show differential block depending on pulse duration when probed by sodium [5], indicating earlier and later open states. This

differential block is not observed in heteromeric I_{Ks} channels, suggesting that multiple open states are not present. However, probing I_{Ks} channels with rubidium results in sigmoidal deactivation [6], which indicates at least two open states. One way to reconcile these results is to assume that the transition from the first open state to the second open state is relatively rapid. Under these conditions, the first open state would not be detected by sodium block, because the transition would be too rapid to be seen experimentally; however, sigmoidal deactivation would still be possible. Our I_{Ks} model is derived from macroscopic data that indicate a faster transition into the open state and slower deactivation, and requires two open states to reproduce steady-state current. The transition rate between O_1 and O_2 in our model is relatively rapid ($\tau << 200$ ms) and would not have been detected by the sodium block experiments. Thus the model is in agreement with the hypothesis put forward by Pusch et al [5] to reconcile rubidium and sodium block experiments.

Pusch et al [6] have also observed that a flickery block is responsible for KCNQ1 inactivation. This flickery block affects all channel states, but is facilitated when the channel enters a later open state (farther from the closed state; [7]. During a depolarizing pulse channels enter the later open state, allowing more inactivation [6,7]. Our model only allows inactivation from a single open state. Flickery block from other channel states is accounted for by introducing a lower macroscopic conductance in our simulations.

Fitting Model Parameters

Simulated KCNQ1 activation was compared to biexponential fits (equation below) to experimental current traces at different voltages provided by M. Sanguinetti.

$$I_{Activation} = A_1 \cdot \exp\left(\frac{t}{\tau_1}\right) + A_2 \cdot \exp\left(\frac{t}{\tau_2}\right)$$

Where A_1 and A_2 are the amplitudes of the exponentials and τ_1 and τ_2 are the time constants for activation.

Channels were assumed to be closed at -80 mV; therefore instantaneous (leak) current was subtracted so that there was no current at time zero. Deactivation ($I_{Deactivation}$) at -70 mV was fit to data reconstructed from published [4] mean values of steady-state inactivation, recovery from inactivation, activation and time constant of deactivation according to the following equation:

$$I_{Deactivation} = Activation(V_m) \cdot \exp\left(-\frac{t}{\tau_{Deactivation}}\right) - Inactivation(V_m) \cdot \exp\left(-\frac{t}{\tau_{Recovery}}\right)$$

Where:

Activation is the percentage of channels open at V_m (-70 mV).
t is time (ms).
$\tau_{Deactivation}$ is the time constant of deactivation.
Inactivation is the percentage of channels inactivated at V_m (-70 mV).
$\tau_{Recovery}$ is the time constant for recovery from inactivation.

Simulated time constants of inactivation and deactivation were measured by fitting exponentials with the Nelder-Mead simplex algorithm[8]. Peak current in the triple pulse protocol was normalized to steady-state current at 40 mV.

In KCNQ1 experiments, relative inactivation is used to measure the percentage of activated channels that become inactivated. This measurement is especially useful for KCNQ1 because channels only partially inactivate. Relative inactivation is measured at the beginning of the tail current as 1-x/y, where x is initial tail current and y is extrapolated current (found by fitting a single exponential to tail current). The extrapolated current measures what the tail current would be if no channels were inactivated during the depolarizing pulse. In our simulations (shown in **Figure 2E** in the paper), x corresponds to $\sum_{i=1}^{5} O_i$ (the sum of the open states at the initial tail current); y is $\sum_{i=1}^{5} O_i + I$ at the same point in time, (I is the inactivated state). Thus, the expression used to find relative

inactivation using the model is $1-\frac{\sum_{i=1}^{5} O_i}{\sum_{i=1}^{5} O_i + I}$, or one minus the ratio of open state occupancy to sum of open state and inactivated state occupancy.

Oocyte experiments by Tristani-Firouzi and Sanguinetti [4] isolate various channel properties, allowing specific transitions to be fit. Activation current traces at many different potentials (**Figure 2A**, in the paper) constrain the parameters describing the closed-state forward transition rates α, γ and the voltage-independent transition, θ. The two time constants of activation described in the results section of the paper (fast and slow) each have an associated weight that is determined by the closed-state occupancy at rest, which in turn is governed by the magnitude of the forward rate relative to the magnitude of the reverse rate at the resting potential. Thus, the steady-state occupancy of the closed states at rest constrains β and δ at negative potentials. The voltage dependence and magnitude of λ are determined by the time constant of inactivation at different voltages (**Figure 2C and 2D**, of the paper). Finally, the peak current, which reflects the steady-state inactivation during the depolarizing pulse, constrains the value of μ at positive potential, while at negative potential it is constrained by the rate of recovery from inactivation (hook, **Figure 2A** of the paper).

Similar to KCNQ1, published I_{Ks} current traces were fit with biexponentials, leak current was subtracted, and steady-state values were normalized to experimental average. The fitting procedure relies on experiments that display the important channel properties including the time-course of activation (including delay), steady-state current-voltage relationship, rate of deactivation and accumulation during pacing. The forward rate transitions, α and γ, were constrained by activation current traces to different potentials. The closed state occupancy that determines the delay before activation, constrains β and δ as in KCNQ1. These transitions also affect I_{Ks} accumulation during pacing, which is within the experimental range (see results section in paper). Deactivation was also included in the optimization and constrains the reverse open state transitions, η and ω. These transitions and the forward state transitions, θ and ψ, are also affected by the steady-state I-V relationship. The predictive ability of the model was verified by its ability to reproduce AP morphology, APD rate-dependent adaptation over the entire range of physiological frequencies, and frequency independent APD prolongation with a drug model that uses an experimentally measured off-rate [9].

Parameters for both KCNQ1 and I_{Ks} models were estimated using the Nelder-Mead simplex algorithm [8] and Asynchronous Parallel Pattern Search [10]. Optimization and simulations were performed on a cluster with fifty-two 2.8 GHz Intel Xeon processors.

Action Potential Simulations

For AP simulations, sets of differential equations describing the I_{Ks}, I_{Kr}, and I_{Na} Markov models were solved using a 4th order Rosenbrock method with Shampine parameters [11]. All variables were scaled to a maximum probability of 1 and absolute error was set not to exceed 10^{-6}. The maximum step size was limited to 0.1 ms and was decreased to 0.01 before the stimulus. The Markov model requiring the smallest step determined the time step used to solve all equations. Calcium dynamics, pumps, exchangers, and background currents are from the LRd model [12-14] available at http://rudylab.wustl.edu.

Extracellular concentrations were set to $[Na^+]_o$=136 mM, $[K^+]_o$=5.4 mM, and $[Ca^{2+}]_o$=2 mM, while intracellular concentrations varied dynamically. Temperature was always set to 37 ºC to match experimental conditions in Bosch et al[15], with the exception of KCNQ1 channels, which were simulated at 23 ºC because sufficient body temperature data were not available. These concentrations and temperature were maintained for all simulations to allow for comparison. Cells were kept quiescent for 10 min to achieve steady-state resting conditions before all protocols.

Action potential duration (APD) was measured at 90% repolarization to V_{rest} (recorded immediately before stimulus) from peak V_m with time zero at dV_m/dt_{max}. The stimulus applied was -80 μA/μF for 0.5 ms

KCNQ1 Rates (ms^{-1})

$$I_{KCNQ1} = \overline{G_{KCNQ1}} \cdot O_{KCNQ1} \cdot (V_m - E_{Ks})$$

Where maximum conductance, $\overline{G_{KCNQ1}}$, is:

$$\overline{G_{KCNQ1}} = 0.054 \cdot \left(1 + \frac{0.6}{1 + \left(\frac{3.8 \cdot 10^{-5}}{\left[Ca^{2+} \right]_i} \right)^{1.4}} \right)$$

← **Accounts for dependence of conductance on intracellular calcium concentration $[Ca^{2+}]_i$[16].**

and open probability, O:

$$O_{KCNQ1} = O_1 + O_2 + O_3 + O_4 + O_5$$

$$E_{Ks} = \frac{R \cdot T}{F} \cdot \log \frac{[K^+]_o + P_{Na/K} \cdot [Na^+]_i}{[K^+]_i + P_{Na/K} \cdot [Na^+]_i}$$

$$\alpha = 9.57 \cdot 10^{-4} \cdot \exp(1.98 \cdot 10^{-1} \cdot \frac{V_m \cdot F}{R \cdot T})$$

$$\beta = 5.00 \cdot 10^{-5} \cdot \exp(-3.33 \cdot 10^{-2} \cdot \frac{V_m \cdot F}{R \cdot T})$$

$$\gamma = 3.77 \cdot 10^{-2} \cdot \exp(3.33 \cdot 10^{-2} \cdot \frac{V_m \cdot F}{R \cdot T})$$

$$\delta = 4.77 \cdot 10^{-2} \cdot \exp(-4.77 \cdot 10^{-1} \cdot \frac{V_m \cdot F}{R \cdot T})$$

$$\theta = 7.98 \cdot 10^{-2}$$

$$\eta = 2.06 \cdot 10^{-2} \cdot \exp(-1.04 \cdot \frac{V_m \cdot F}{R \cdot T})$$

$$\psi = 2.54 \cdot 10^{-2} \cdot \exp(6.46 \cdot 10^{-2} \cdot \frac{V_m \cdot F}{R \cdot T})$$

$$\omega = 1.78 \cdot 10^{-2} \cdot \exp(-5.32 \cdot 10^{-1} \cdot \frac{V_m \cdot F}{R \cdot T})$$

$$\lambda = 2.32 \cdot 10^{-2} \cdot \exp(1.21 \cdot 10^{-1} \cdot \frac{V_m \cdot F}{R \cdot T})$$

$$\mu = 6.19 \cdot 10^{-2} \cdot \exp(-9.46 \cdot 10^{-2} \cdot \frac{V_m \cdot F}{R \cdot T})$$

$$\nu = -9.00 \cdot 10^{1}$$

$$x_\psi = \exp(z_\psi \cdot (z_\psi + z_\omega) \cdot \nu \cdot \frac{F}{RT})$$

$$x_\omega = \exp(z_\omega \cdot (z_\psi + z_\omega) \cdot \nu \cdot \frac{F}{RT})$$

$$\psi_n = \psi \cdot x_\psi^{n-1}$$

$$\omega_n = \omega \cdot x_\omega^{n-1}$$

Guinea Pig I_{Ks} Rates (ms^{-1})

$$I_{Ks} = \overline{G_{Ks}} \cdot O_{Ks} \cdot (V_m - E_{Ks})$$

$$\overline{G_{Ks}} = 0.2165 \cdot \left(1 + \frac{0.6}{1 + \left(\frac{3.8 \cdot 10^{-5}}{\left[Ca^{2+} \right]_i} \right)^{1.4}} \right)$$

$$O_{Ks} = O_1 + O_2$$

$$E_{Ks} = \frac{R \cdot T}{F} \cdot \log \frac{[K^+]_o + P_{Na/K} \cdot [Na^+]_i}{[K^+]_i + P_{Na/K} \cdot [Na^+]_i}$$

$$\alpha = 3.72 \cdot 10^{-3} \cdot \exp(2.10 \cdot 10^{-1} \cdot \frac{V_m \cdot F}{R \cdot T})$$

$$\beta = 2.35 \cdot 10^{-4} \cdot \exp(-2.42 \cdot 10^{-1} \cdot \frac{V_m \cdot F}{R \cdot T})$$

$$\gamma = 7.25 \cdot 10^{-3} \cdot \exp(2.43 \cdot 10^{0} \cdot \frac{V_m \cdot F}{R \cdot T})$$

$$\delta = 1.53 \cdot 10^{-3} \cdot \exp(-6.26 \cdot 10^{-1} \cdot \frac{V_m \cdot F}{R \cdot T})$$

$$\theta = 1.96 \cdot 10^{-3}$$

$$\eta = 1.67 \cdot 10^{-2} \cdot \exp(-1.34 \cdot 10^{0} \cdot \frac{V_m \cdot F}{R \cdot T})$$

$$\psi = 3.41 \cdot 10^{-4} \cdot \exp(1.24 \cdot 10^{0} \cdot \frac{V_m \cdot F}{R \cdot T})$$

$$\omega = 2.62 \cdot 10^{-4} \cdot \exp(-8.07 \cdot 10^{-1} \cdot \frac{V_m \cdot F}{R \cdot T})$$

Human I_{Ks} Rates (ms^{-1})

$$I_{Ks} = \overline{G_{Ks}} \cdot O_{Ks} \cdot (V_m - E_{Ks})$$

$$\overline{G_{Ks}} = 0.779 \cdot \left(1 + \frac{0.6}{1 + \left(\frac{3.8 \cdot 10^{-5}}{\left[Ca^{2+} \right]_i} \right)^{1.4}} \right)$$

$$O_{Ks} = O_1 + O_2$$

$$E_{Ks} = \frac{R \cdot T}{F} \cdot \log \frac{[K^+]_o + P_{Na/K} \cdot [Na^+]_i}{[K^+]_i + P_{Na/K} \cdot [Na^+]_i}$$

$$\alpha = 3.98 \cdot 10^{-4} \cdot \exp(3.61 \cdot 10^{-1} \cdot \frac{V_m \cdot F}{R \cdot T})$$

$$\beta = 5.74 \cdot 10^{-5} \cdot \exp(-9.23 \cdot 10^{-2} \cdot \frac{V_m \cdot F}{R \cdot T})$$

$$\gamma = 3.41 \cdot 10^{-3} \cdot \exp(8.68 \cdot 10^{-1} \cdot \frac{V_m \cdot F}{R \cdot T})$$

$$\delta = 1.20 \cdot 10^{-3} \cdot \exp(-3.30 \cdot 10^{-1} \cdot \frac{V_m \cdot F}{R \cdot T})$$

$$\theta = 6.47 \cdot 10^{-3}$$

$$\eta = 1.25 \cdot 10^{-2} \cdot \exp(-4.81 \cdot 10^{-1} \cdot \frac{V_m \cdot F}{R \cdot T})$$

$$\psi = 6.33 \cdot 10^{-3} \cdot \exp(1.27 \cdot 10^{0} \cdot \frac{V_m \cdot F}{R \cdot T})$$

$$\omega = 4.91 \cdot 10^{-3} \cdot \exp(-6.79 \cdot 10^{-1} \cdot \frac{V_m \cdot F}{R \cdot T})$$

Guinea Pig I_{Kr} (Rapid Delayed Rectifier) Model

A previous Markov model of guinea pig I_{Kr} [17] was updated. Simulations generated by the revised model are compared to the current-voltage relationship (**Figure A1-A**), activation (**Figure A1-B**), and rectification (**Figure A1-C**) measured by Sanguinetti and Jurkiewicz [18]. Current-voltage relationship was measured at the end of a 550 ms pulse to various potentials and activation was the sum of the occupancy in the open and inactivated states at the end of the same pulse. Rectification was reproduced with a 225 ms pulse to various potentials and calculated as the occupancy in the open state over the sum of the occupancy of the open and inactivated states, O/(O+I). Currents simulated for a 550 ms pulse are shown in **Figure A1-D**. The updated model was also able to reproduce recent experiments by Rocchetti et al [19] (**Figure A1-E and A1-F**). Consistent with AP-clamp experimental observations, peak current during the AP does not increase significantly as rate increase. However, in simulations I_{Kr} is greater at the start and during the plateau of the AP (**Figure A1-E and A1-F**) than in the experiment. Increasing rectification to decrease early I_{Kr} led to conflicting results with rectification experiments [18]. A possible explanation to this conflict is an observation by Gurrola et al [20] that ErgTx, which was used in the AP clamp experiments, is inhibited at higher membrane potentials [20], which would cause underestimation at the beginning of the AP. Furthermore, ErgTx does not block inactivated channels, resulting in underestimation of current contribution as channels recover from inactivation during the plateau of the AP.

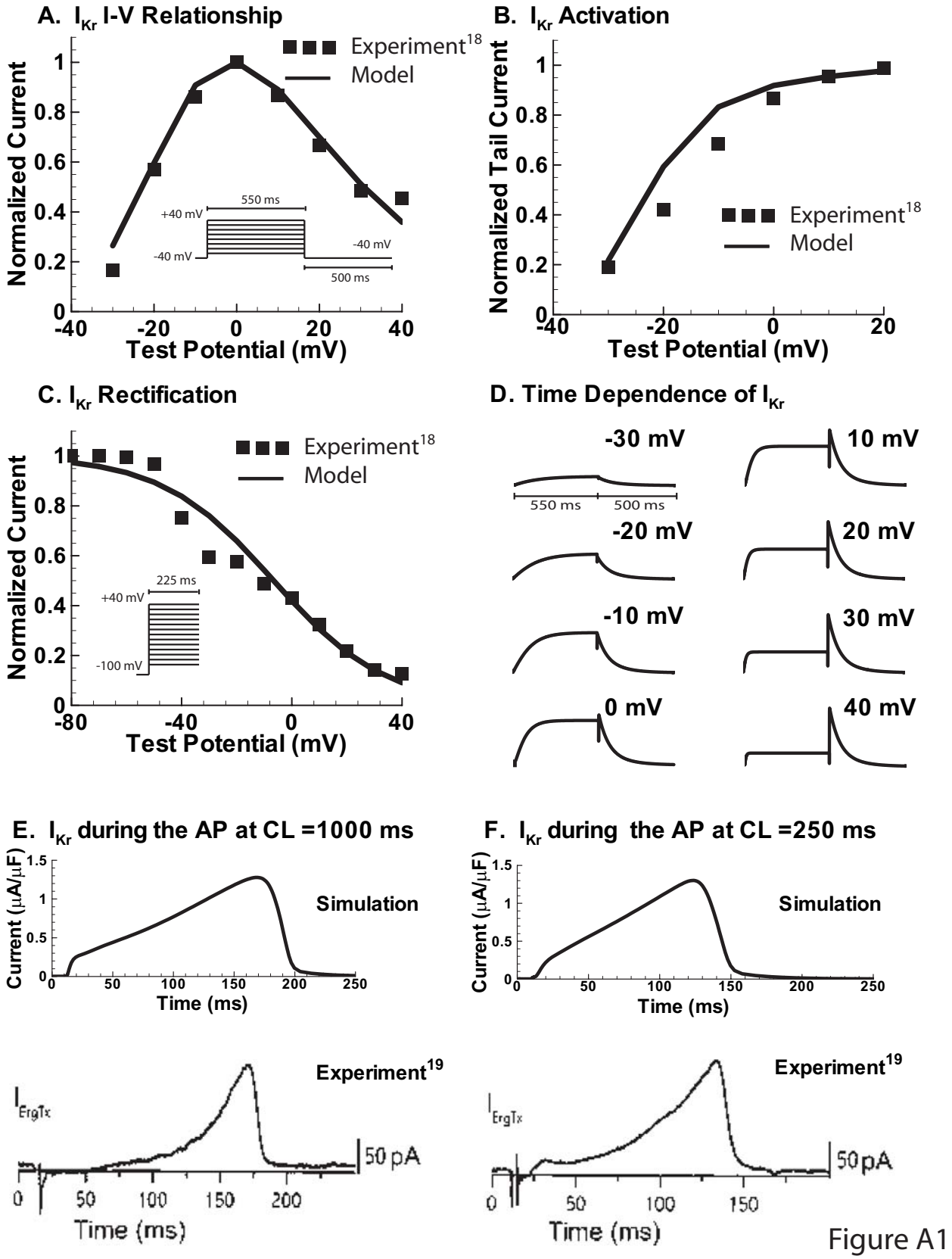
A. I_{Kr} I-V Relationship
Experiment[18]
Model
Normalized Current
Test Potential (mV)
550 ms
+40 mV
-40 mV
-40 mV
500 ms
B. I_{Kr} Activation
Normalized Tail Current
Experiment[18]
Model
Test Potential (mV)
C. I_{Kr} Rectification
Experiment[18]
Model
Normalized Current
225 ms
+40 mV
-100 mV
Test Potential (mV)
D. Time Dependence of I_{Kr}
-30 mV
550 ms
500 ms
10 mV
-20 mV
20 mV
-10 mV
30 mV
0 mV
40 mV
E. I_{Kr} during the AP at CL =1000 ms
Current (μA/μF)
Simulation
Time (ms)
Experiment[19]
I_{ErgTx}
50 pA
Time (ms)
F. I_{Kr} during the AP at CL =250 ms
Current (μA/μF)
Simulation
Time (ms)
Experiment[19]
I_{ErgTx}
50 pA
Time (ms)

Figure A1

Figure A1: Simulations of I_{Kr}. I_{Kr} was fit to experimental data from Sanguinetti and Jurkiewicz [18]. Protocol used to obtain Current-Voltage (I-V) relationship (Panel A) and Activation (Panel B) is shown in inset of panel A. Rectification (Panel C) was measured using a step from -100 mV to various potentials. The current traces generated by the protocol shown in A are shown in Panel D. Panels E and F show I_{Kr} during the action potential at CL= 1000 ms (Panel E) and CL = 250 ms (Panel F). Simulated currents are shown above, and the experimentally observed ErgTx sensitive current is shown below [19].

I_{Kr} Markov Model

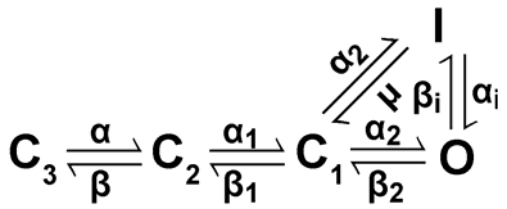

I_{Kr} Equations

$$I_{Kr} = \overline{G_{Kr}} \cdot O_{Kr} \cdot (V_m - E_{Kr})$$

O_{Kr} is the open probability

$$\overline{G_{Kr}} = 0.0135 \cdot [K^+]_o^{0.59}$$

$$E_{Kr} = \frac{R \cdot T}{F} \cdot \log \frac{[K^+]_o}{[K^+]_i}$$

$$\alpha_2 = 1.31 \cdot 10^{-2} \cdot \exp(1.48 \cdot 10^{0} \cdot \frac{V_m \cdot F}{R \cdot T})$$

$$\beta_2 = 3.30 \cdot 10^{-3} \cdot \exp(-5.77 \cdot 10^{-1} \cdot \frac{V_m \cdot F}{R \cdot T})$$

$$\alpha_1 = 2.17$$

$$\beta_1 = 1.08$$

$$\alpha = 3.02 \cdot 10^{-2} \cdot \exp(1.48 \cdot 10^{0} \cdot \frac{V_m \cdot F}{R \cdot T})$$

$$\beta = 2.90 \cdot 10^{-3} \cdot \exp(-9.78 \cdot 10^{-1} \cdot \frac{V_m \cdot F}{R \cdot T})$$

$$\alpha_i = 5.45 \cdot 10^{-1} \cdot \exp(-8.17 \cdot 10^{-1} \cdot \frac{V_m \cdot F}{R \cdot T}) \cdot \frac{4.5}{[K^+]_o}$$

$$\beta_i = 8.20 \cdot 10^{-1} \cdot \exp(5.04 \cdot 10^{-1} \cdot \frac{V_m \cdot F}{R \cdot T}) \cdot (\frac{4.5}{[K^+]_o})^3$$

$$\mu = \alpha_i \cdot \beta_2 \, / \, \beta_i$$

References

1. Zagotta WN, Hoshi T, Aldrich RW. Shaker potassium channel gating. III: Evaluation of kinetic models for activation. *J Gen Physiol*. 1994;103:321-62.
2. Koren G, Liman ER, Logothetis DE, Nadal-Ginard B, Hess P. Gating mechanism of a cloned potassium channel expressed in frog oocytes and mammalian cells. *Neuron*. 1990;4:39-51.
3. Pusch M, Magrassi R, Wollnik B, Conti F. Activation and inactivation of homomeric KvLQT1 potassium channels. *Biophys J*. 1998;75:785-92.
4. Tristani-Firouzi M, Sanguinetti MC. Voltage-dependent inactivation of the human K+ channel KvLQT1 is eliminated by association with minimal K+ channel (minK) subunits. *J Physiol*. 1998;510 (Pt 1):37-45.
5. Pusch M, Ferrera L, Friedrich T. Two open states and rate-limiting gating steps revealed by intracellular Na+ block of human KCNQ1 and KCNQ1/KCNE1 K+ channels. *J Physiol*. 2001;533:135-43.
6. Pusch M, Bertorello L, Conti F. Gating and flickery block differentially affected by rubidium in homomeric KCNQ1 and heteromeric KCNQ1/KCNE1 potassium channels. *Biophys J*. 2000;78:211-26.
7. Seebohm G, Sanguinetti MC, Pusch M. Tight coupling of Rubidium conductance and inactivation in human KCNQ1 potassium channels. *J Physiol*. 2003.
8. Nelder JA, Mead R. A Simplex Method for Function Minimization. *Computer Journal*. 1965;7:313.
9. Fujisawa S, Ono K, Iijima T. Time-dependent block of the slowly activating delayed rectifier K(+) current by chromanol 293B in guinea-pig ventricular cells. *Br J Pharmacol*. 2000;129:1007-13.
10. Hough PD, Kolda TG, Torczon VJ. Asynchronous Parallel Pattern Search for Nonlinear Optimization. *SIAM Journal on Scientific Computing*. 2001;23:134-156.
11. Press WH, Numerical Recipes Software (Firm). Numerical recipes in C. In. 2nd ed., v2.0. ed. [Cambridge, England] ; [New York, N.Y.]: Cambridge University Press,; 1993.
12. Faber GM, Rudy Y. Action potential and contractility changes in [Na(+)](i) overloaded cardiac myocytes: a simulation study. *Biophys J*. 2000;78:2392-404.
13. Zeng J, Laurita KR, Rosenbaum DS, Rudy Y. Two components of the delayed rectifier K+ current in ventricular myocytes of the guinea pig type. Theoretical formulation and their role in repolarization. *Circ Res*. 1995;77:140-52.
14. Luo CH, Rudy Y. A dynamic model of the cardiac ventricular action potential. I. Simulations of ionic currents and concentration changes. *Circ Res*. 1994;74:1071-96.
15. Bosch RF, Gaspo R, Busch AE, Lang HJ, Li GR, Nattel S. Effects of the chromanol 293B, a selective blocker of the slow, component of the delayed rectifier K+ current, on repolarization in human and guinea pig ventricular myocytes. *Cardiovasc Res*. 1998;38:441-50.

16. Viswanathan PC, Shaw RM, Rudy Y. Effects of IKr and IKs heterogeneity on action potential duration and its rate dependence: a simulation study. *Circulation*. 1999;99:2466-74.
17. Clancy CE, Rudy Y. Cellular consequences of HERG mutations in the long QT syndrome: precursors to sudden cardiac death. *Cardiovasc Res*. 2001;50:301-13.
18. Sanguinetti MC, Jurkiewicz NK. Two components of cardiac delayed rectifier K+ current. Differential sensitivity to block by class III antiarrhythmic agents. *J Gen Physiol*. 1990;96:195-215.
19. Rocchetti M, Besana A, Gurrola GB, Possani LD, Zaza A. Rate dependency of delayed rectifier currents during the guinea-pig ventricular action potential. *J Physiol*. 2001;534:721-32.
20. Gurrola GB, Rosati B, Rocchetti M, Pimienta G, Zaza A, Arcangeli A, Olivotto M, Possani LD, Wanke E. A toxin to nervous, cardiac, and endocrine ERG K+ channels isolated from Centruroides noxius scorpion venom. *Faseb J*. 1999;13:953-62.